Near-IR- and UV-femtosecond laser waveguide inscription in silica glasses

VINCENZO DE MICHELE,[1,2,*] MAXIME ROYON,[1] EMMANUEL MARIN,[1] ![ORCID] ANTONINO ALESSI,[1] ADRIANA MORANA,[1] AZIZ BOUKENTER,[1] MARCO CANNAS,[2] SYLVAIN GIRARD,[1] AND YOUCEF OUERDANE[1] ![ORCID]

[1]*Univ-Lyon, Laboratoire Hubert Curien (LabHC), CNRS UMR 5516, 18 Rue Pr. Benoit, 42000 Saint-Etienne, France*
[2]*Università degli Studi di Palermo, Dipartimento di Fisica e Chimica, Palermo I-90123, Italy*
[*]*vincenzo.demichele@univ-st-etienne.fr*

Abstract: The influence of laser parameters on silica based waveguide inscription is investigated by using femtosecond laser pulses at 1030 nm (near-IR) and at 343 nm (UV). Negative phase contrast microscopy technique is used to measure the refractive index contrast for different photo-inscribed waveguides and shows the effects of both laser wavelength and scanning speed. In particular, UV photons have a higher efficiency in the waveguide production process as also confirmed by the lower optical losses at 1550 nm in these waveguides. These measurements are combined with micro-Raman and photoluminescence techniques, highlighting that laser exposure induces both structural modification of the silica and point defects generation. The contribution of induced defects to the total refractive index change is singled out by applying two different thermal treatments on the waveguide. The first, up to 500 °C, is able to remove the most of the induced non-bridging-oxygen-hole-centers (NBOHCs) while the second up to 750 °C erases almost all absorbing induced defects, highlighting the strong contribution of additional defects, not yet identified.

1. Introduction

The development of high intensity femtosecond (fs) pulsed lasers has given a strong boost to the production of efficient and innovative devices in the field of photonics [1]. Combining the high collimation with the improvements of the chirped pulse amplification technique [2], ultrafast laser manufacturing takes advantage of the very high peak intensity (~10 TW/cm^2) to induce permanent structural modifications in transparent materials, such as silica glasses. These changes lead to a refractive index variation along laser's path that can be controlled with a high spatial resolution, adjusting the laser fluence at µm and sub-µm scales [3]. Such adjustment is crucial for the inscription of optical waveguides or more complex 3D photonic structures [4–8]. The employment of these devices remains limited by their optical losses, so process parameters should also be optimized to reduce them as much as possible [9].

The improvement of the light guiding properties is strongly related to the contrast control of the induced refractive index change. To this purpose, the effect of the different laser exposure conditions on the waveguides inscription must be characterized. In general, in silica glasses exposed to fs laser pulses it is possible to produce two regimes of interaction: Type I, at relatively low pulses energies, and Type II at higher pulse energy [10,11]. Type I is characterized by isotropic positive refractive index change. Glass densification and point defects creation are observed along the inscription path. For Type II, the strong temperature increase of the focal point drives the inscription to thermo-mechanical expansion of the material with a negative refractive index change, leading in certain conditions to void formations.

The effects of the laser scanning speed, temporal pulse width, pulse shape, repetition rate, beam profile, laser polarization and focusing conditions were widely investigated in the past years [12–16]. Nowadays there is a lack of investigations on the impact of the choice for the laser wavelength on the waveguide properties. Even if neglected in the past, the laser wavelength plays a key role in the waveguide inscription using direct laser writing techniques, especially in the control of the refractive index change. The importance of the present topic is highlighted by a very recently publication whose authors studied, through experimental and numerical simulation investigations, the wavelength dependence of the size of the laser-inscribed tracks, the structural modifications, the damage and the waveguides writing energy dependence [17].

The purpose of the present work is the investigation of the laser wavelength choice in direct inscription of waveguides inside bulk silica. The resulting waveguides, inscribed in the UV-domain and in the near-IR as function of the scanning speed and the energy per pulse, will be characterized in terms of induced modifications of the silica network and defects creation. The structural modifications of the photo-inscribed waveguides are studied through Raman technique, highlighting the different effects in the network reorganization, due to the wavelength choice. In this way is possible to have information on the induced densification dependence on laser wavelengths. The created defects are investigated via photoluminescence (PL) and the refractive index contrast by the phase contrast microscopy technique. Furthermore, we studied the optical properties of the manufactured waveguides, estimating experimentally the refractive index difference between the waveguides and the pristine glass and the optical losses. In order to gain more information on the nature of the induced refractive index change, the samples were submitted to two selectively thermal treatments, in order to anneal the photo-induced defects, in particular NBOHC. The goal of this thermal treatment is to provide us an evaluation of the defects contribution to the total induced refractive index variation.

2. Experimental description

Sample under test is a polished Herasil 1 ($10\times10\times4$ mm^3), natural glass produced by flame fusion of quartz crystal. In the Brückner classification [18], this glass is a "Type II" silica, with OH content of about 150-400 ppm (in weight) and some germanium impurities, of the order of 1 ppm.

The two laser wavelengths, 1030 nm and 343 nm, are generated by a Yb:KGW femtosecond laser (Light Conversion PHAROS) whose fundamental wavelength is centered at 1030 nm with a pulse duration about ~200 fs and a repetition rate of 100 kHz. Coupling the Pharos laser with a harmonic generator (Light Conversion HIRO), it is possible to obtain femtosecond laser pulses in the UV range, centered at 343 nm. The corresponding temporal pulse width is about 200 fs. A polarizer coupled with a half-wave plate drove the power control, and since the inscription was performed in transverse geometry, a slit was employed to guarantee a cylindrical profile of the inscribed waveguides [19,20]. Laser pulses were focused 200 μm below the bulk surface by microscope objectives with a nominal numerical aperture (NA) of 0.42 and 0.5, respectively for the laser wavelengths at 1030 nm and 343 nm. By moving the sample thanks to a XYZ computer-controlled stage (AEROTECH), it is possible to write a waveguide inscription of 9 mm in length with 8 passes. In addition, to the evaluation of the impact of the laser wavelength choice on the inscription process, we analyzed the waveguides characteristics as function of the scanning speed (*100 μm/s, 300 μm/s and 600 μm/s*) and of the energy per pulse (*1.20 μJ/pulse and 1.30 μJ/pulse @ 1030 nm and 0.20 μJ/pulse and 0.35 μJ/pulse @ 343 nm*).

In order to probe local structural modifications and the defects induced by the femtosecond pulses irradiation, the integrated confocal micro-spectrometer ARAMIS (Horiba Jobin-Yvon) was used in a backscattering configuration. This system is equipped with a He-Cd laser (325 nm) acting as the probing laser for both the PL and Raman measurements. Sample was mounted on an XYZ controlled stage (micrometric precision) and the beam focalized with a 40× UV

objective. The microRaman parameters were chosen to achieve a spatial resolution (in the XY plane) of ~5 μm thanks to a confocal pinhole of 50 μm of diameter. All the Raman data have been acquired with 2400 lines/mm grating with a spectral resolution of ~5 cm^{-1}.

The refractive index contrasts of the corresponding waveguides, compared to the pristine glass, were measured using a negative phase contrast microscopy (ZEISS AXIO microscopy) in transmission configuration.

A white light source (350 nm and 2000 nm) allowed us studying the optical properties of the inscribed waveguides, as the mode confinement and the estimation of the refractive index change. This last parameter was roughly evaluated by measuring the NA of the output light mode in far-field configuration, using a CMOS camera (Thorlabs DCC1645C). Knowing the NA of the waveguides, the refractive index change Δn is calculated by the relation NA = $\sqrt{2n\Delta n}$.

The waveguide losses at 1550 nm have been evaluated by using an optical backscatter reflectometer (OBR 4600) from Luna technologies, which records the backscattered Rayleigh signal along the waveguide length by sweeping the laser wavelength in a small range of ~ 40 nm centered at 1550 nm. The choice of these parameters allowed us to obtain a spatial resolution of ~20 μm.

3. Results and discussion

3.1. PL and Raman measurements

The energy deposition of femtosecond laser pulses drives the generation of free electron plasma in the focal volume. During the plasma relaxation, the hot electrons transfer their energy to the ions, resulting in different types of structural modification. In our experimental conditions (Type I regime of interaction), smooth positive isotropic refractive index changes are induced by defect-assisted structural changes. In the following, the induced modifications inside the glass are investigated via PL and Raman measurements.

Figure 1, at left, shows the PL spectra, with laser probe excitation at 325 nm, of the pristine sample (red line) and the waveguide inscribed at 0.20 μJ/pulse, 100 μm/s @ 343 nm (black line). This comparison reveals the presence of a PL band peaked at 650 nm in the sample exposed to femtosecond laser pulses. This spectral feature is well known and attributed to the point defects called NBOHC. These defects are also commonly observed in irradiated silica-based materials [21,22].
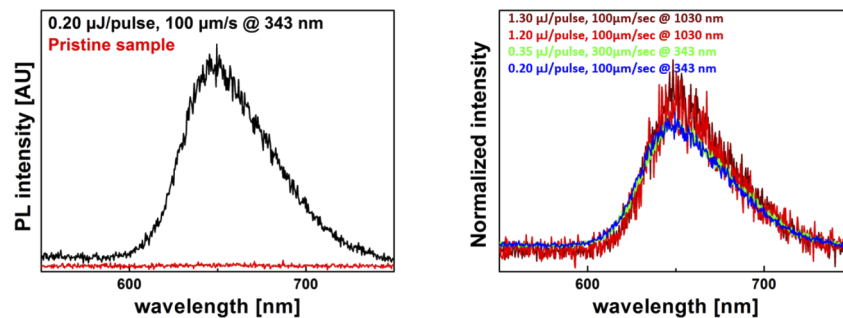

Fig. 1. At left, the comparison between the PL spectra of the pristine sample (red line) and the PL spectra of the waveguide inscribed using 0.20 μJ/pulse, 100 μm/s @ 343 nm. At right the normalized PL spectra of different waveguides: dark red line at 1.30 μJ/pulse, 100 μm/s @ 1030 nm, red line at 1.20 μJ/pulse, 100 μm/s @ 1030 nm, green line at 0.35 μJ/pulse, 300 μm/s @ 343 nm and the blue line at 0.20 μJ/pulse, 100 μm/s @ 343 nm.

Figure 1, at right, shows the normalized (respect to the total area) PL responses of different waveguides inscribed in the same glass at different wavelengths and experimental conditions.

Neglecting the different signal-noise ratio, all the spectra manifest the same spectral feature, confirming that the NBOHC creation is a characteristic feature of the Type I interaction regime, resulting a mark of smooth positive refractive index change induced by femtosecond laser pulses deposition.

The most widely accepted picture of the NBOHC generation is related to the free carrier trapping, after the plasma generation, as the Self-Trapped Excitons (STXs) [23], leading to stress and consequently breakage of the Si-O bonds. The broken bond results in the formation of the E' and NBOHC paramagnetic centers [21,23], or could also result in the release of the oxygen leading to Oxygen Deficiency Centers I (ODCs I) formation [23]. The stochastic nature of the defects generation, assisted by the OH groups present in the pristine sample, drives the lattice into a microscopic network reorganization, resulting in a macroscopic (detectable) densification, bounded to the formation of small sized rings.

In order to probe the matrix relaxation after the interaction with the laser, Raman measurements were performed on the inscribed waveguides. Figure 2(a) compares the spectra before/after the laser exposure, highlighting the most important Raman features of the silica glasses.
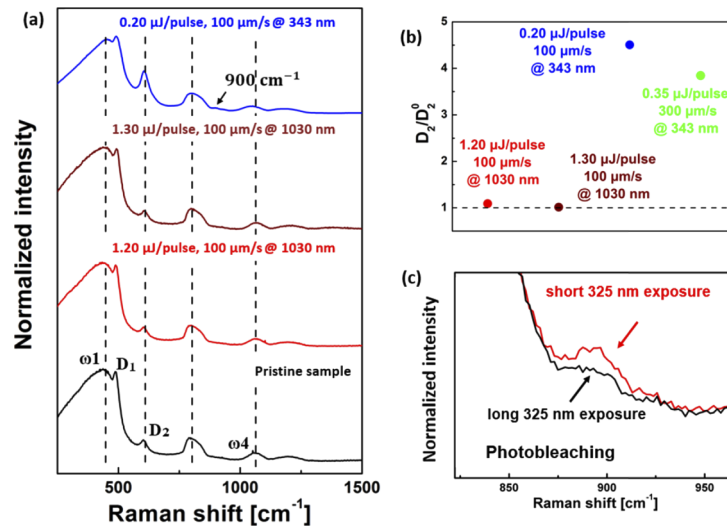

Fig. 2. (a) Comparison between the Raman spectra measured in the pristine sample (black line) and in the waveguides inscribed with the following conditions: dark red line at 1.30 μJ/pulse, 100 μm/s @ 1030 nm, red line at 1.20 μJ/pulse, 100 μm/s @ 1030 nm and the blue line at 0.20 μJ/pulse, 100 μm/s @ 343 nm. (b) Ratio between the areas of the D_2 band of the inscribed waveguides and of the pristine sample (D_2^0). (c) Photo-bleaching investigation of the NBOHC 325 nm resonant band at 896 cm^{-1}: comparison between long (black line) and short (red line) laser exposure.

The main band $\omega 1$ at 440 cm^{-1}, is linked to the oxygen vibration along the Si-O-Si angle bisector of the high-membered rings [24]. The breathing vibration of the 4-membered and 3-membered rings respectively generates the D_1 and D_2 bands, at 490 cm^{-1} and 605 cm^{-1}.

Network reorganization brings to the increase of the number of such few atoms membered rings and also to the densification of the material [25,26]. Even the $\omega 4$ LO-TO (Longitudinal and transversal optical) doublet centered at 1130 cm^{-1} is a feature of structural modification, linked to the asymmetrical stretching of the Si-O-Si bond. By the comparison between the Raman spectra of the waveguides inscribed using the laser in the UV domain with the one of the pristine sample, are evident strong structural modifications, footprint of densified material. For instance the blue shift of the main band, from 440 cm^{-1} to 453 cm^{-1}, is a signature of the decrease of the

Si-O-Si angle in the high-membered rings, also observed in the redshift of the LO-TO doublet, from 1130 cm^{-1} to 1110 cm^{-1} (the minimum in the center of the doublet). The opposite trend of the $\omega 1$ and the $\omega 4$ LO-TO could be explained by their different dependence on the Si-O-Si angle.

In any case, the most evident feature of the network compaction under femtosecond laser pulses is the increase of the concentration of the 3-membered rings observable with the D_2 band area increase. Another footprint of the densification should be the increase of the 4-membered rings through the increase of the D_1 band amplitude; however, due to the overlap of the $\omega 1$ band, any estimation of its variation is very difficult.

Differently, the comparison between the waveguides inscribed at 1030 nm and the pristine sample reveals no densification features or other signature of structural modifications. This is clear in Fig. 2(b) in which we studied the ratio between the areas of the D_2 band of the inscribed waveguides and of the pristine sample (D_2^0). The D_2/D_2^0 ratio of the near-IR waveguides is of the order of 1 while it is higher for the waveguides inscribed at 343 nm.

Moreover we also observed, in the Raman spectra acquired for the waveguide written with at 343 nm laser and pulse energy of 0.2 µJ, the laser-induced band at 896 cm^{-1}: this band was observed in other samples under different classes of irradiations [27,28]. Following the Ref. [29], this feature is assigned to the resonant Raman band of NBOHC at 325 nm. In agreement with this hypothesis, the band is absent with Raman probing laser at 442 nm, but it could be also photo-bleached under long 325 nm exposure as shown in Fig. 2(c) [29]. For the near-IR waveguides, despite the presence of NBOHC PL band, the band at 896 cm^{-1} was not clearly observed.

Ultimately, the Raman comparison between waveguides inscribed with the two wavelengths reveals that notwithstanding the lower energy per pulse adopted using the 343 nm laser wavelength, larger induced modifications are observed in terms of defects creation and densification.

3.2. Optical properties

The defects assisted densification, observed with the spectroscopic characterization of the inscribed waveguides, is coherent with the Type I regime of interaction, which produces isotropic smooth positive refractive index change. Type I enables the light guiding into the inscribed traces. At higher energies per pulse, it is possible to produce Type II structures, characterized by a negative refractive index change. Thermo-mechanical expansion and an intense PL band peaked at 545 nm (not yet definitively attributed to a defect structure) are characteristic of these kinds of traces [10,11].

In order to probe the guiding properties of the waveguides, we studied the increase in the refractive index contrast through phase contrast microscopy (PCM) imaging, as shown in Fig. 3. It is important to keep in mind that in these PCM measurements black colors correspond to positive refractive index changes and white to negative ones.

At fixed energy per pulse, the higher refractive index contrast is measured for the lower scanning speed. In this case at 100 µm/s, and at different energies (and fixed wavelength), there are stronger modifications for the waveguides inscribed at higher laser fluence, even if there is the Type I/Type II threshold. Indeed, the waveguide inscribed at 0.35µJ/pulse, 100 µm/s @ 343 nm is already Type II, while the one inscribed at 1.30 µJ/pulse, 100 µm/s @ 1030 nm is at the limit of the Type I/Type II threshold, manifesting some periodical structures along the trace, losing in this way its isotropic characteristic. Moreover, the comparison between the samples produced with different laser wavelengths shows that higher refractive index contrasts are present in the waveguides inscribed in the UV domain. This is coherent with the modifications, in terms of defects creation and structural changes, observed through the various spectroscopic techniques.

Figure 4 represents the near-field normalized large-band guided mode of the inscribed waveguides. The mode is more confined in the waveguides inscribed using the laser in the UV domain, resulting in better guiding properties under different experimental conditions, compared
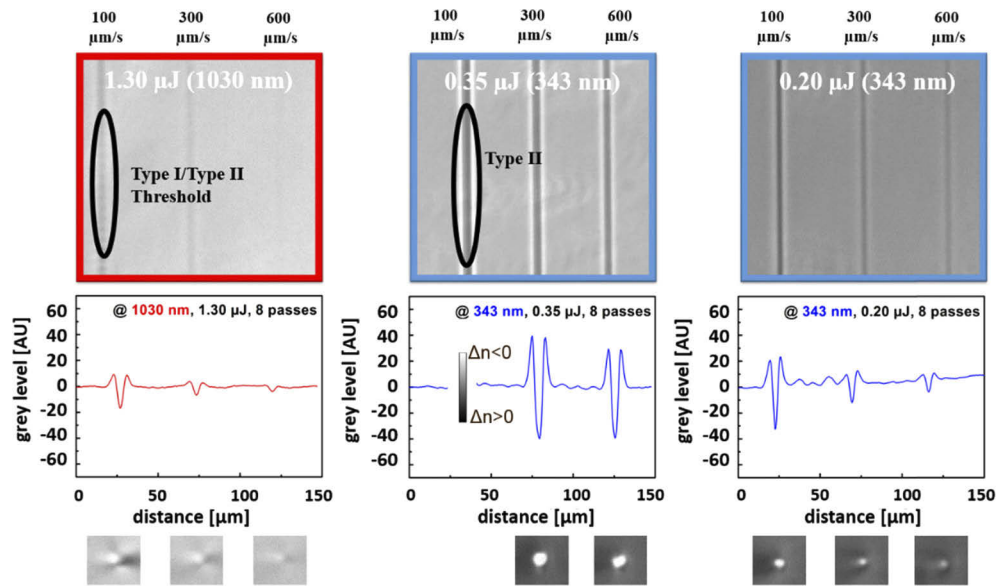
Fig. 3. PCM images as function of scanning speed of the waveguides inscribed with the following experimental conditions: left at 1.30 µJ/pulse @ 1030 nm, in the center at 0.35 µJ/pulse and at right at 0.20 µJ/pulse both @ 343 nm. Below are shown the corresponding refractive index contrasts in grey levels with the relative cross sections.

to the transmitted mode of the waveguides inscribed at 1030 nm, whose confinement is strongly dependent on the writing parameters.
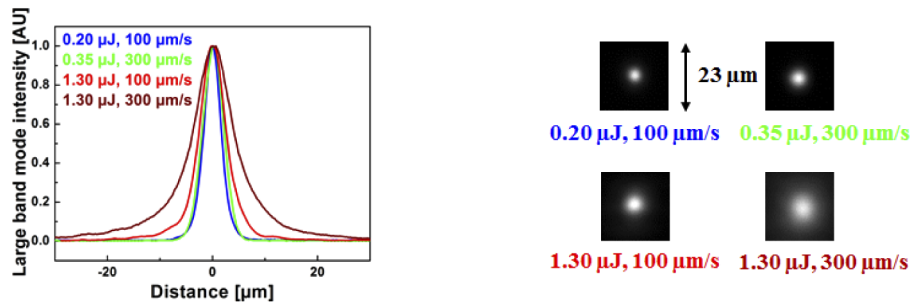

Fig. 4. Normalized large band mode (left), with the corresponding measured spot at the output of the waveguides (right), of the inscribed waveguides at 0.20 µJ/pulse, 100 µm/s @ 343 nm in blue, 0.35 µJ/pulse, 300 µm/s @ 343 nm in green, 1.30 µJ/pulse, 100 µm/s @ 1030 nm in red and 1.30 µJ/pulse, 300 µm/s @ 343 nm in dark red line.

Moreover, we have measured the losses of the waveguides at 1550 nm, representing the third telecommunication window, crucial in case of fiber-waveguides coupled based devices. The OBR measurements give a transmittion losses of the injected light in the range between 0.9 dB/cm and 1.2 dB/cm for near-IR waveguides, in agreement with the results of [30], and between 0.4 dB/cm and 0.6 dB/cm for the UV waveguides.

To have a qualitative evaluation of the benefits of waveguide manufacturing using UV laser, we compare in Fig. 5 the experimentally estimated refractive index change as function of the scanning speed of the inscribed waveguides, with the corresponding value reported in Table 1. Measurements are based on the estimation of the NA, injecting light directly into the waveguides,

acquiring the far field mode waist at different distances. In this way, by the relation NA = $\sqrt{2n\Delta n}$ it is possible to estimate the induced refractive index change [28]. The obtained value should be interpreted as an average index change over the whole VIS-NIR range and along the cross section of the inscribed waveguides, without any pretense of being an exact value of Δn, but only an estimation.
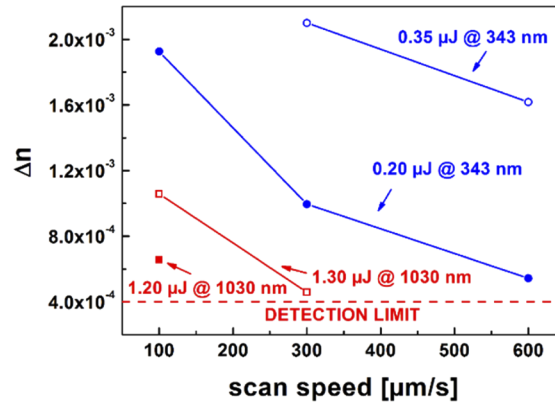

Fig. 5. Measured refractive index changes as function of the scanning speed for the different waveguides: empty blue circles inscribed at 0.35 μJ/pulse @343 nm, full blue circles at 0.20 μJ/pulse @ 343 nm, empty red squares at 1.30 μJ/pulse @ 1030 nm and full red squares at 1.20 μJ/pulse @ 1030 nm. Values with Δn lower than $4 \cdot 10^{-4}$ are below our detection limit.

Table 1. Refractive index changes of the inscribed waveguides.

Scanning speed (μm/s)	1030 nm		343 nm	
	1.20 μJ/pulse	1.30 μJ/pulse	0.20 μJ/pulse	0.35 μJ/pulse
100	$6.6 \cdot 10^{-4}$	$1.1 \cdot 10^{-3}$	$1.9 \cdot 10^{-3}$	Type II
300	Detection limit	$4.6 \cdot 10^{-4}$	$1.0 \cdot 10^{-3}$	$2.1 \cdot 10^{-3}$
600	Detection limit	Detection limit	$5.4 \cdot 10^{-4}$	$1.6 \cdot 10^{-3}$

From Fig. 5, we can appreciate the higher refractive index change induced in the silica by the 343 nm laser, even at lower fluencies, highlighting the better efficiency of the inscription process. Another evidence in Fig. 5 is the strong difference between the Type I/Type II thresholds in the different structures.

It is important to notice that in the present work we are comparing the efficiency of the induced refractive index contrast during the inscription and not the maximum obtained value. Indeed, using different experimental conditions, it is possible to obtain Δn comparable or higher, eg. by using 800 nm femtosecond laser pulses [28]. The explanation of this efficiency could be linked to the different energies of the absorbed photons: the multiphoton ionization, that is the main process for the plasma generation, requires ~3 photons at 343 nm and ~8 at 1030 nm, making the non-linear absorption much efficient in the UV domain, as already observed in [31].

3.3. Thermal treatment

Since in the silica glass the positive refractive index change could be induced by densification (Lorentz-Lorenz relation) and through the presence of new absorption bands (Kramers-Kronig relations), we performed a thermal treatment to our samples, in order to anneal the induced defects. The comparison of the refractive index contrast of the waveguides before and after the

thermal treatment allows the estimation of the induced point defects contribution to the total refractive index contrast.

The first thermal treatment (TT 1) consists of sample annealing until 500 °C (20 min). 500°C is a temperature for which the NBOHC defects should be bleached [22]. The second treatment, up to 750 °C (20 min), ensures the annealing of almost all the induced defects [32]. After a cooling down to RT, we have compared the refractive index contrast, in gray levels, of the waveguides before and after the treatments. The results comparison is shown in Fig. 6.
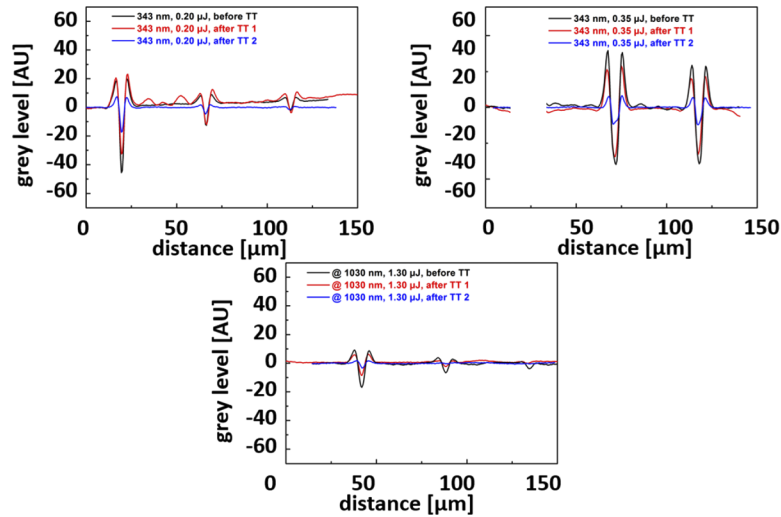

Fig. 6. Comparison between the refractive index contrasts in grey level of the waveguides before (black line) and after the thermal treatments (TT1 in red and TT2 in blue). For each graph, the waveguide at left is inscribed at 100 μm/s, in the center at 300 μm/s and at right at 600 μm/s.

Starting from the TT 1 (red line in Fig. 6), for waveguides inscribed in the UV domain, the ratio between the refractive index contrast before and after the thermal treatment is around 1. With a similar treatment, it is possible to reduce the losses of the waveguides, bleaching the absorbing defects, without huge changes in the induced positive refractive index change. Differently, in the case of the waveguides inscribed using the laser at 1030 nm, the ratio between the refractive index contrast before and after the thermal treatment is of the order of 2, highlighting a larger contribution of the defects to the induced Δn. These kinds of waveguides are more sensitive to the increasing temperature. Indeed, by the second thermal treatment (blue line in Fig. 6), these waveguides are almost erased. It is clear that the contribution of the non-NBOHC defects is even stronger compared to these ones, which are the only defects detectable with the PL or Raman measurements. From the TT1 seems that the Δn is driven by the densification for the waveguides inscribed with the 343 nm laser, while through the second thermal treatment is evident that the defects play an important role to the total refractive index change. Indeed, considering the NBOHC formation as results of the STX decay, the complementary formation of the E' defects could be suggested, as already observed in waveguides inscribed using fs laser pulses at 800 nm [33]. Furthermore, as supposed by [23], ODC (I) formation could be a consequence of the STX decay. Figure 6 highlights the needs for further studies with additional experimental techniques to discriminate between the different defects responsible of the annealed contribution observed in TT2.

4.   Conclusions

In the present work we have studied the laser wavelength effects on the waveguide inscription, using femtosecond laser pulses at 1030 nm and 343 nm. By comparing the spectroscopic characteristics of the different waveguides, we have observed more important structural modifications in the waveguides inscribed with UV laser pulses. This leads also to stronger light guiding properties. Moreover, there is higher efficiency in the refractive index change induced by the UV laser: at lower energies per pulse, higher positive refractive index changes are induced compared to 1030 nm laser case. There is also a difference in the Type I/Type II threshold at the two different laser wavelengths. For instance, the waveguides inscribed with the near-IR laser reach the Type II before to attain Δn comparable with those of waveguides inscribed at 343 nm. This is not a general rule, since different experimental conditions could provide similar Δn using 800 nm femtosecond pulses [28]. In conclusion, to estimate the contribution of the defects to the Δn with respect the densification, we have submitted our written waveguides to two thermal treatments: the first temperature, 500°C, was chosen to anneal almost all the NBOHCs, while the second one, at 750°C, was selected to anneal almost all the laser-induced absorbing defects. By comparing the refractive index contrasts of the waveguides before and after the first thermal treatment, no noticeable difference is observed for the UV photo-inscribed waveguides. For the near-IR waveguides, it is interesting to note that, notwithstanding the absence of densification evidences (with Raman measurements), these waveguides survive to the thermal treatment, with a less important Δn. This means that the induced defects (in particular NBOHC) strongly contribute to the index change. The second thermal treatment almost erased the waveguides inscribed using near-IR laser, clarifying the defects-dependent nature of these structures, coupled with a very soft densification. The second thermal treatment highlights the strong contribution of other defects than NBOHC to the refractive index contrast for the waveguides inscribed at 343 nm. Further measurements are needed and will be performed in the future to clarify the nature and structure of these defects.

Disclosures

The authors declare no conflict of interest.

References

1. R. R. Grattas and E. Mazur, "Femtosecond laser micromachining in transparent materials," Nat. Photonics **2**(4), 219–225 (2008).
2. D. Strickland and G. Mourou, "Compression of amplified chirped optical pulses," Opt. Commun. **56**(3), 219–221 (1985).
3. M. Ali, T. Wagner, M. Shakoor, and P. Molian, "Review of laser nanomachining," J. Laser Appl. **20**(3), 169–184 (2008).
4. E. N. Glezer, M. Milosavljevic, L. Huang, R. J. Finlay, T.-H. Her, J. P. Callan, and E. Mazur, "Three-dimensional optical storage inside transparent materials," Opt. Lett. **21**(24), 2023–2025 (1996).
5. N. Jovanovic, P. G. Tuthill, B. Norrin, S. Gross, P. Steward, N. Charles, S. Lacour, M. Ams, J. S. Lawrence, A. Lehmann, C. Niel, J. G. Robertson, G. D. Marshall, M. Ireland, A. Fuerbach, and M. J. Withford, "Starlight demonstration of the Dragonfly instrument: an integrated photonic pupil-remapping interferometer for high-contrast imaging," Mon. Not. R. Astron. Soc. **427**(1), 806–815 (2012).
6. M. Royon, D. Piétroy, E. Marin, and A. Saoulot, "A thermomechanical sensor using photo-inscribed volume Bragg gratings," Tribol. Int. **115**, 417–423 (2017).
7. Y. Sikorski, A. A. Said, P. Bado, R. Maynard, C. Florea, and K. A. Winick, "Optical waveguide amplifier in nd-doped glass written with near-IR femtosecond laser pulses," Electron. Lett. **36**(3), 226–227 (2000).
8. G. Della Valle, S. Taccheo, R. Osellame, A. Festa, G. Cerullo, and P. Laporta, "1.5 μm single longitudinal mode waveguide laser fabricated by femtosecond laser writing," Opt. Express **15**(6), 3190–3194 (2007).
9. S. Gross and M. J. Withford, "Ultrafast-laser-inscribed 3D integrated photonics: challenges and emerging applications," Nanophotonics **4**(3), 332–352 (2015).
10. K. M. Davis, K. Miura, N. Sugimoto, and K. Hirao, "Writing waveguides in glass with femtosecond laser," Opt. Lett. **21**(21), 1729–1731 (1996).

11. Y. Shimotsuma, P. Kazansky, J. Qiu, and K. Hirao, "Self-organized Nanogratings in glass irradiated by Ultrashort light," Phys. Rev. Lett. **91**(24), 247405 (2003).
12. B. C. Stuart, M. D. Feit, A. M. Rubenchik, B. W. Shore, and M. D. Perry, "Laser-induced damage in dielectrics with nanosecond to subpicosecond pulses," Phys. Rev. Lett. **74**(12), 2248–2251 (1995).
13. B. Poumellec, M. Lancry, A. Chahid-Erraji, and P. G. Kazansky, "Dependence of the femtosecond laser refractive index change thresholds on the chemical composition of doped-silica glasses," Opt. Mater. Express **1**(4), 766–782 (2011).
14. I. M. Burakov, N. M. Bulgakova, R. Stoian, A. Mermillod-Blondin, E. Audouard, A. Rosenfeld, A. Husakou, and I. V. Hertel, "Spatial distribution of refractive index variations induced in bulk fused silica by single ultrashort and short laser pulses," J. Appl. Phys. **101**(4), 043506 (2007).
15. C. B. Schaffer, A. Brodeur, and E. Mazur, "Laser-induced breakdown and damage in bulk transparent materials induced by tightly focused femtosecond laser pulses," Meas. Sci. Technol. **12**(11), 1784–1794 (2001).
16. V. V. Temnov, K. Sokolowki-Tinten, P. Zhou, A. El-Khamhawy, and D. von der Linde, "Multiphoton ionization in dielectrics: comparison of circular and linear polarization," Phys. Rev. Lett. **97**(23), 237403 (2006).
17. J. H. Rueda, J. Clarijs, D. van Ooste, and D. M. Krol, "The influence of femtosecond laser wavelength on waveguides fabrication inside fused silica," Appl. Phys. Lett. **110**(16), 161109 (2017).
18. R. Brückner, "Properties and structures of vitreous silica," J. Non-Cryst. Solids **5**(2), 123–175 (1970).
19. M. Ams, G. D. Marshall, D. J. Spence, and M. J. Withford, "Slit beam shaping method for femtosecond laser direct-write fabrication of symmetric waveguides in bulk glasses," Opt. Express **13**(15), 5676–5681 (2005).
20. Y. Cheng, K. Sugioka, K. Midorikawa, M. Masuda, K. Toyoda, M. Kawachi, and K. Shihoyama, "Control of the croos-sectional shape of a hollow microchannel embedded in photostructurable glass by the use of a femtosecond lase," Opt. Lett. **28**(1), 55–57 (2003).
21. L. Skuja, "Optical properties of defects in silica," in: G. Pacchioni, L. Skuja, and D. L. Griscom, eds., "Defects in related dielectrics: science and technology" (NATO Science Series II), (Kluwer, 2000), pp. 73–116
22. A. Morana, M. Cannas, S. Girard, A. Boukenter, L. Vaccaro, J. Périsse, J.-R. Macé, Y. Ouerdane, and R. Boscaino, "Origin of the visible absorption in radiation-resistant optical fibers," Opt. Mater. Express **3**(10), 1769 (2013).
23. A. L. Sluger, "The model of a triplet self-trapped exciton in crystalline SiO_2," J. Phys. C: Solid State Phys. **21**(13), L431–L434 (1988).
24. D. M. Krol, "Femtosecond laser modification of glass," J. Non-Cryst. Solids **354**(2-9), 416–424 (2008).
25. G. S. Henderson, D. R. Neuville, B. Cochain, and L. Cormier, "Structural change of GeO_2-SiO_2 glasses and melt: a Raman spectroscopy study," J. Non-Cryst. Solids **355**(8), 468–474 (2009).
26. J. W. Chan, T. Huser, S. Risbud, and D. M. Krol, "Structural change in fused silica after exposure to focused femtosecond laser pulses," Opt. Lett. **26**(21), 1726–1728 (2001).
27. M. Léon, L. Giacomazzi, S. Girard, N. Richard, P. Martín-Samos, A. Ibarra, A. Boukenter, and Y. Ouerdane, "Neutron irradiation effects on the structural properties of KU1, KS-4 V and I301 silica glasses," IEEE Trans. Nucl. Sci. **61**(4), 1522–1530 (2014).
28. M. Royon, E. Marin, S. Girard, A. Boukenter, Y. Ouerdane, and R. Stoian, "X-ray preconditioning for enhancing refractive index contrast in femtosecond laser photoinscription of embedded waveguides in pure silica," Opt. Mater. Express **9**(1), 65–74 (2019).
29. D. Di Francesca, A. Boukenter, S. Agnello, A. Alessi, S. Girard, M. Cannas, and Y. Ouerdane, "Resonance raman of oxygen dangling bonds in amorphous silicon dioxide," J. Raman Spectrosc. **48**(2), 230–234 (2017).
30. Y. Zhang, C. Lin, C. Liao, K. Yang, Z. Li, and Y. Wang, "Femtosecond laser-inscribed fiber interface Mach-Zehnder interferometer for temperature-insensitive refractive index measurements," Opt. Lett. **43**(18), 4421–4424 (2018).
31. M. Cavillon, M. Lancry, B. Poumellec, Y. Wang, J. Canning, K. Cook, T. Hawkings, P. Dragic, and B. Ballato, "Overview of high temperature fiber bragg gratings and potential improvement using highly doped aluminosilicate glass optical fibers," J. Phys. Photonics **1**(4), 042001 (2019).
32. A. Saliminia, J.-P. Bérubé, and R. Vallée, "Refractive index-modified structures in glass written by 266 nm fs laser pulses," Opt. Express **20**(25), 27410–27419 (2012).
33. A. M. Streltsov and N. F. Borrelli, "Study of femtosecond-laser-written waveguides in glasses," J. Opt. Soc. Am. B **19**(10), 2496–2504 (2002).